final thesis without ftir and interaction TURNITIN.pdf

Datta Meghe Institute of Medical Sciences, Wardha

Document Details

Submission ID
trn:oid:::27005:142438906

Submission Date
Jun 10, 2026, 3:24 PM GMT+5:30

Download Date
Jun 10, 2026, 3:30 PM GMT+5:30

File Name
final thesis without ftir and interaction TURNITIN.pdf

File Size
1.2 MB

44 Pages

8,132 Words

45,153 Characters

7% Overall Similarity

The combined total of all matches, including overlapping sources, for each database.

Filtered from the Report

- Bibliography
- Quoted Text
- Cited Text
- Small Matches (less than 18 words)

Match Groups

19 Not Cited or Quoted 7%
Matches with neither in-text citation nor quotation marks

0 Missing Quotations 0%
Matches that are still very similar to source material

0 Missing Citation 0%
Matches that have quotation marks, but no in-text citation

0 Cited and Quoted 0%
Matches with in-text citation present, but no quotation marks

Top Sources

5% Internet sources
5% Publications
4% Submitted works (Student Papers)

Integrity Flags

0 Integrity Flags for Review

No suspicious text manipulations found.

Our system's algorithms look deeply at a document for any inconsistencies that would set it apart from a normal submission. If we notice something strange, we flag it for you to review.

A Flag is not necessarily an indicator of a problem. However, we'd recommend you focus your attention there for further review.

Match Groups

- **19** Not Cited or Quoted 7%
  Matches with neither in-text citation nor quotation marks
- **0** Missing Quotations 0%
  Matches that are still very similar to source material
- **0** Missing Citation 0%
  Matches that have quotation marks, but no in-text citation
- **0** Cited and Quoted 0%
  Matches with in-text citation present, but no quotation marks

Top Sources

5% Internet sources
5% Publications
4% Submitted works (Student Papers)

Top Sources

The sources with the highest number of matches within the submission. Overlapping sources will not be displayed.

1	Internet	
coek.info		<1%
2	Submitted works	
Delhi Technological University on 2026-04-09		<1%
3	Internet	
www.mdpi.com		<1%
4	Submitted works	
Birzeit University Main Library on 2021-11-05		<1%
5	Submitted works	
Higher Education Commission Pakistan on 2023-06-18		<1%
6	Internet	
assets-eu.researchsquare.com		<1%
7	Submitted works	
Higher Education Commission Pakistan on 2023-08-15		<1%
8	Submitted works	
Visvesvaraya National Institute of Technology on 2021-05-13		<1%
9	Publication	
Anmol Kumar, Shubhangi Pandey, Krishna Kumar, S. Krishnamoorthi, Kranthiku...		<1%
10	Internet	
books.rsc.org		<1%

11 Internet

biointerfaceresearch.com <1%

12 Publication

B.S. Bibin, Pethurajan Vigneshwaran, K. John Samuel, Aabid Hussain Shaik, Gunda... <1%

13 Publication

Deepshikha Hazarika, Berileena Hazarika. "Cellulose-based stimuli-responsive an... <1%

14 Submitted works

University of College Cork on 2025-10-10 <1%

15 Internet

storage.googleapis.com <1%

16 Internet

www.tandfonline.com <1%

17 Publication

Prashant Sahu, Sushil K. Kashaw, Varsha Kashaw, J.P. Shabaaz, Rajiv Dahiya. "Basi... <1%

18 Publication

H.N. Jayasimha, K.G. Chandrappa, P.F. Sanaulla, V.G. Dileepkumar. "Green synthe... <1%

CHAPTER 1

INTRODUCTION AND LITERATURE SURVEY

INTRODUCTION

Hydrogels are high water content, 3D networks of natural or synthetic polymers, with a high degree of flexibility[1]. They are ideal for use in a wide range of applications because they are soft, rubber-like, have a consistency similar to living tissues, and can hold a significant amount of water or biological fluids under physiological conditions. A hydrogel is sometimes referred to as a "smart" or "intelligent" material because it can sense stimuli and react by changing its chemical or physical characteristics, which causes the trapped drug to release under controlled conditions [2].

The presence of hydrophilic groups like -OH, -CONH, -SO_3H and -$CONH_2$ in polymers that form hydrogel structures is responsible for their propensity to absorb water. Depending on the type, the polymer is thus hydrated to varying degrees (sometimes more than 90%wt.) due to the contribution of these groups and domains in the network.[2], [3]. The hydrophilic functionalities cross-linking offers structural stability and keeps the hydrophilic polymers from dissolving in the aqueous medium right away [4].

Important properties of hydrogels include stretchability, deformability, biocompatibility, softness, and toughness. Polymer-based hydrogels have found widespread application in drug delivery, food, cosmetics, contact lenses, corneal implants, tendons, ligaments, cartilage, and bone due to their exceptional hydrophilicity, permeability, compatibility, and low friction coefficient. Additionally, superporous hydrogels, a unique class of hydrogels, may find use as superdisintegrants, controlled release platforms, and gastroretentive drug delivery systems in both short- and long-term applications [5]. Here, we'll concentrate on oral medication delivery.

1.1. Classification of Hydrogel:

Hydrogels have been classified into following different groups based on their origin, structure, preparation method, crosslinking mechanism, charge, responsive nature, physical aspect, and degradation.[6]

Fig 1 represents a broad classification of hydrogels formulated based on a literature survey.

- **Based on source**

Hydrogels can be broadly categorized into three groups based on their source: natural, semi-synthetic and synthetic.

a) **Natural hydrogels**- provides biocompatibility.
b) **Semi-synthetic hydrogels**- which have adjustable characteristics.
c) **Synthetic hydrogel**- which offers a high degree of variability.[7]

- **Based on Composition**

The composition of hydrogels can be used to classify them into four categories, viz., homopolymeric, copolymeric, interpenetrating polymer network (IPN), and semi interpenetrating polymer network hydrogels (semi-IPN)

a) **Homopolymer Hydrogel**- The polymeric chains homopolymer hydrogel are derived from one species of monomer.[8]
b) **Copolymer hydrogels**- Copolymeric hydrogels are made up of two or more distinct monomer species with at least one hydrophilic component that are arranged along the polymer network's chain in an alternating, random, or block pattern.[9]
c) **Interpenetrating Polymer Network (IPN)-** A polymer made up of two or more networks that are at least partially molecularly interlaced but not covalently bonded to one another, making it impossible to separate them without breaking chemical bonds. An IPN is not a combination of two or more pre-formed polymer networks [10], [11]
d) **Semi- Interpenetrating Polymer Network-** A polymer made up of one or more networks and one or more linear or branched polymers, where at least some of the linear or branched macromolecules penetrate at least one of the networks on a molecular scale.[11], [12]

- **Based on Configuration**

Based on their configuration, hydrogels are divided into three groups. Depending on how they are arranged, hydrogels can be amorphous, crystalline, or semi-crystalline.[3]

a) **Amorphous-** An amorphous polymer's molecular structure is entirely random, meaning that its molecular chains are entangled and oriented randomly with no discernible pattern.[13], [14]
b) **Crystalline-** The long range order is present in the crystalline structure.[15]
c) **Semi-crystalline-** Both crystal line and amorphous phases make up semicrystalline polymers. Because they contain crystalline regions, their mechanical performance at high temperatures is frequently better than that of amorphous polymers.[16], [17]

- **Based on Cross-linking**

Depending on whether the cross-link junctions are chemical or physical, hydrogels can be classified into two groups.

a) Chemically cross-linked networks- have permanent junctions.

b) **Physical networks**- have transient junctions that are caused by either polymer chain entanglements or physical interactions like hydrogen bonds, ionic interactions, or hydrophobic interactions.[8]

- **Based on Ionic- Charge**

Based on whether there is an electrical charge on the cross-linked chains, hydrogels can be divided into four groups

a) Nonionic (neutral).
b) Ionic (including cationic or anionic).
c) Amphoteric electrolyte (ampholytic) that has both basic and acidic groups.
d) Zwitterionic (polybetaines) which have cationic and anionic groups in each structural repeating unit.[18]

- **They are categorized according to the mechanism governing the release of drugs:**

a) Systems with diffusion-controlled release.

b) Systems for swelling controlled release.

c) Systems with chemically regulated release.

d) Systems that respond to the environment.

CMTKG:

Tamarind Kernel Gum (TKG), which is extracted from Tamarindus indica L seeds, is the source of CMTKG, a biopolymer. This polysaccharide is composed of galactose, xylose, and glucose in a 3:2:1 ratio. Its linear β-(1,4)-D glucose backbone has partial α-D-xylo-pyranose (C-1) substitution at the O glucopyranosyl (C-6) residues, which are then further substituted at C-2 by β-D galactopyranosyl units (C-1). Williamson's etherification (SN 2 mechanism) of TKG

and alkaline mono-chloroacetic acid results in CMTKG, which has carboxymethyl groups (-CH2COOH) at its C-6 position [19].

Carboxymethyl tamarind kernel gum (CMTKG), which has appropriate properties like broad pH tolerance, high drug loading capacity, hydrophilicity, and stability, is produced by chemically modifying TKG [20]

The antibacterial qualities of TKG are demonstrated by CMTKG. Tissue engineering, drug delivery, agriculture, paper, and textiles are just a few of the industries that can benefit from CMTKG's superior functional qualities. Over the past ten years, a thorough investigation into CMTKG as a drug delivery method has been conducted due to reliable data regarding its excellent pharmacological and physicochemical properties [21].

Bovine Serum Albumin (BSA):

With 76% similarity, BSA and HSA are the most frequently used protein models in biophysical and biochemical research in recent years [22].

11 According to the crystal structure analysis, BSA contains 582 amino acid residues, 20 tyrosyl residues (Tyr), and two tryptophan residues (Try), which are located in positions 134 (sub domain IA) and 212 (sub-domain IIA) [23].

The water-soluble nature of bovine serum albumin (BSA), which is crucial for interaction studies, has led to its selection[24] [22].

Numerous mononuclear and polynuclear Cu2+, Ni2+, Zn2+, Co2+, and Pt2+ complexes with aromatic ligands—some of which have known pharmacologically active moieties—have been studied for their BSA interaction and binding capacity.[22]

Polyacrylamide:

PAM is composed of repeating units of the acrylamide (AM)[25]. The non-toxic, pH-sensitive polymer polyacrylamide (PAM) is well known for its exceptional biocompatibility. It has the –CONH2 group, which allows for flexible swelling and drug release behaviors at various pH levels.[26]

PAM-based hydrogels exhibit mechanical resilience and the ability to maintain their shape. To create composite hydrogels with exceptional qualities, they have been widely mixed with synthetic and natural polymers like carboxymethyl cellulose and carboxymethyl tamarind kernel gum. [27]

Poly(acrylic acid):

Acrylic acid polymerises to form Poly(acrylic acid). The following equation illustrates how the PAA chains can absorb and hold onto water molecules when water at neutral pH is present because they will lose their protons and gain a negative charge, [28]

$$n\ CH_2=CH-CO_2H+H_2O \xrightarrow{pH=7.0} n\ CH_2=CH-H_2O+COOH \quad (1)$$

Madagascar periwinkle plant:

Vinca rosea, Ammocallis rosea, and Lochnera rosea are some synonyms for Catharanthus roseus L. It is a significant Apocynaceae medicinal plant with a wealth of beneficial alkaloids that are used to treat menstrual issues, diabetes, blood pressure, asthma, constipation, and cancer. of thousands of patients, both due to their efficacy and distinct mode of action. The plant has long been used in traditional Chinese medicine, Ayurvedic medicine, and other medical systems. In the 20th century, Western medical researchers started studying Catharanthus roseus and its extracts, discovering a number of compounds that could be used to treat cancer. The dried root, leaves, flowers, and stalks of the plant have all been utilized in local herbal medicine. The entire dried plant is used to extract alkaloids for use in contemporary medicine [29].

MP is available in a wide range of styles and hues, from the original pink to white, hot pink, purple, and mauve [30]

Additionally, we used MP leaves that have purple flowers, or "rosea." Two types of PM—rosea and alba—have been the subject of numerous studies. All of the findings showed that rosea performs better overall than alba. Rosea fared much better under water stress than alba because it has more antioxidant activity and a higher alkaloid content in its leaves and roots [31].

Copper Oxide Nanoparticles:

It is commonly known that the properties of nanoparticles are superior to those of their bulk counterparts. Particle size and specific surface area are inversely correlated. Because of their larger surface area, nanoparticles are therefore used to increase the rates of interfacial processes. As a result, nanoparticles are superior adsorbents and catalysts. With intended uses in numerous scientific and technological domains, the need for nanomaterials is constantly

growing. Green nanomaterial synthesis has garnered a lot of interest. Green synthesis frequently makes use of plant extracts with therapeutic value. Few components of plant extracts with therapeutic value are thought to be included in the synthesis of nanoparticles [32]. We have followed similarly.

CuO NPs amalgamation has been considered superior to other metal oxide nanoparticles due to their enormous potential applications over the past ten year

[33].

Due to their wide range of uses. They have superior antibacterial effects without compromising the material's mechanical qualities because of their higher surface-to-volume ratio and smaller particle size. Co-precipitation, sol-gel, hydrothermal, and other techniques can be used to create copper oxide nanoparticles. These techniques, however, have a number of disadvantages, such as inconsistent particle sizes, the use of dangerous chemicals, high costs, and substantial energy consumption. A simpler, more affordable, and ecologically friendly green synthesis technique that uses plant secondary metabolites as capping agents has been developed to overcome these constraints [34] Through coordination bonds or electron donation, plant functional groups interact with metal ions on the surface of nanoparticles in green synthesis techniques [11]. Capping agents are frequently used in colloidal dispersions to precisely control the growth, agglomeration, and physicochemical properties of nanoparticles. Consequently, their antibacterial activity is enhanced by keeping the particle size within the nanoscale range [34].

Ciprofloxacin:

A second-generation broad-spectrum antibiotic, ciprofloxacin (CFX) exhibits encouraging outcomes because of its improved pharmacokinetic activity and efficient treatment of a number of dangerous infections [35].

CFX is a broad-spectrum antimicrobial fluoroquinolone that is clinically recommended for the treatment of bacterial infections, including infectious diarrhea, typhoid fever, acute uncomplicated cystitis in females, chronic bacterial prostatitis, urinary and lower respiratory tract infections, acute sinusitis and skin-related infections, bone and joint infections, and uncomplicated cervical and urethra gonorrhea. The gastrointestinal tract absorbs it at a high rate. The permeability of this medication varies with concentration[36].

To the best of our knowledge, carboxymethyl tamarind kernel gum (CMTKG) is being used for the first time with BSA and polyacrylamide. This work involves synthesis, characterization,

swelling studies, drug release experiment, and the kinetic modeling of drug released CFX from CuO-loaded CMTKG/BSA/PAM-based hydrogels.

1 Biodegradable polymeric hydrogels are represented as an excellent drug delivery system to fine-tuned drug release profile as per clinical necessity. However, the direct incorporation of drug molecules into the hydrogel matrix has been reported with very high initial burst release profile followed by the short-term slow release profile. In addition, this burst release could go beyond 70% of the total drug loading, consequently, the smaller amount of drug available for the prolonged release. Ultimately, a problem of antibiotic resistance may appear.

This research delves into the fabrication of CFX-loaded CMTKG-g-poly(acrylamide-co-acrylic acid)/BSA/CuO bio-nanocomposite hydrogel, aiming for a pH-dependent, slow and controlled release of the drug CFX.

Characterization techniques such as PXRD, ATR-FTIR, FESEM were employed to assess the hydrogels. Additionally, the study investigates how varying amounts of BSA and CuO NPs have an impact on the hydrogels' swelling behaviour in pH 2.2 and 7.4 buffers. Additionally, a variety of mathematical models, including Korsmeyer-Peppas, Higuchi, Zero order, and First order, were used to assess the drug release kinetics.

LITERATURE SURVEY

Hydrogel Material	Crosslinker	NPs	Drug	Reference
CMTKG/Poly(sodium acrylate)	PEGDA	ZnO	Ciprofloxacin	**[37]**
PAM/MMT/CMC/MgO	MBA	MgO	Acyclovir	**[38]**
CMC and PEG	DA-PEG	Tannic acid	Antagomir-21	**[39]**
Alginate	Cystine/$CaCl_2$	Fe_3CO_4	Doxorubicin	**[40]**
Hyaluronic acid	HS-MMP-SH	Copper Sulphide	Deferoxamine	**[41]**
Guggal gum/PAM	MBA	SrO-CoO	**Naproxen**	**[42]**

CHAPTER 2

MATERIAL AND SYNTHESIS

2.1 Materials

Carboxymethyl tamarind kernel gum (CMTKG) having a molecular weight (MW = 9.14×10^5 g mol^{-1}) was generously provided by Hindustan gum (Bhiwani, India), Acrylamide (AAM), Acrylic Acid (AA), potassium persulphate (KPS) and *N*, *N*′-methylenebisacrylamide (MBA) were received from the Merck, Germany. Distilled water was used for the solution prepration.

2.2. Preparation of Plant Extract

Madagascar periwinkle plant leaves were collected from garden and washed properly to remove the dirt and impurities from the leaves. The leaves were left for drying. Solvent Extraction method was used to get the plant extract. The dried leaves were then emersed in 100 ml of ethanol for around 30 min that was followed by addition of 100 ml water to it. Then the mixture was left for boiling for around 1 hr at 60°C. Later the filteration process was performed using Whatman filter paper. The filtrate was kept in refrigerator at 4-6°C for future use.[43]

2.3. Synthesis of Lysine-coated CuO Bio-Nanoparticles

CuO NPs were effectively produced from Madagascar periwinkle plant extract. 1g of $CuCl_2$ was dissolved in 100 ml distilled water with continuous stirring. NaOH was used to lower down the pH to 10. 20 ml of MP plant extract and 0.4 g lysine was added after 2 hr stirring. The temperature was maintained around 70-85°C. Whatman filter paper used to get the precipitate from filtrate. The precipitate was then washed with a solution of ethanol and distilled water and left for drying in oven for 48h and stored for later use [44]

2.4. Synthesis of **CMTKG-g-poly(acrylamide-co-acrylic acid)/BSA composite hydrogel**

The free radical polymerization technique is used to prepare the CMTKG-BSA-PAM-AA hydrogel network. CMTKG was mixed in 7 ml distilled water and left for dissolution for 1 hr with continuous stirring at 470 rpm. BSA in 2 ml distilled water was then added in dissolved CMTKG solution. 10 min later, acrylamide was added and left for stirring for 30 min. After that acrylic acid was added and after 10 min the KPS was added followed by addition of MBA. Polymerization process was carried out for 20 min. The product was transferred into test tube for hot water bath for 45 min at 80°C. The synthesised hydrogel was then dispersed into distilled water to eliminate the unreacted monomers for 1 hour. After that, the forrmed

hydrogel was left in an incubator for drying [45]. The composition of used substituents is shown in the table below:

Table 1.

Sample Name	Composition Ratio					
	CMTKG	BSA	ACRYLAMIDE	ACRYLIC ACID	MBA	KPS
B0	0.3g	0	0.4g	20µl	0.020g	0.028g
B1	0.3g	0.1g	0.4g	20µl	0.020g	0.028g
B2	0.3g	0.2g	0.4g	20µl	0.020g	0.028g
B3	0.3g	0.3g	0.4g	20µl	0.020g	0.028g

2.5. Preparation of **CMTKG-g-poly(acrylamide-co-acrylic acid)/BSA/CuO nanocomposite hydrogel**

A range of nanocomposite hydrogels were produced by adding various amounts of CuO NPs. CuO NPs were weighed in different quantities- 10 mg and 20 mg and added in the above mentioned procedure with few drops PEG just before the addition of KPS and MBA. [37]. PEG was added for the purpose of dispersion of CuO NPs in the hydrogel [46]

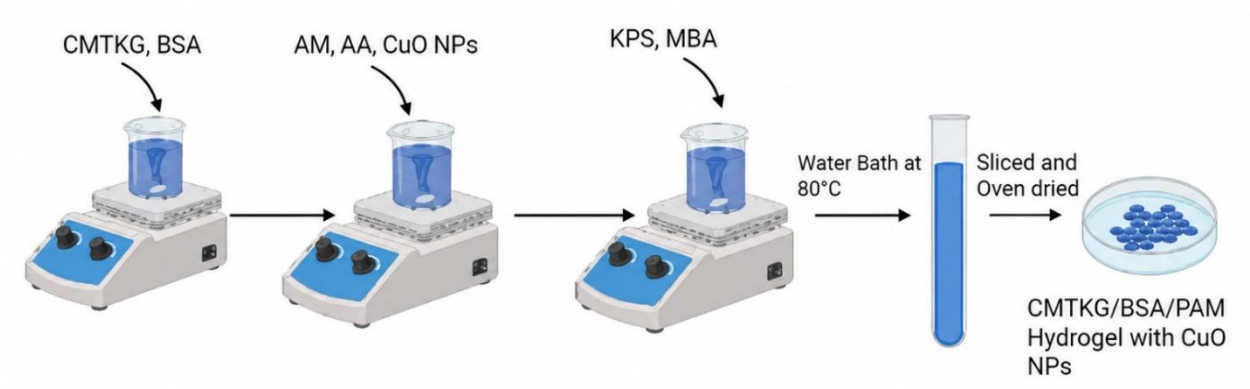

Fig 2.1 Synthesis of CMTKG/BSA/PAM/CuO Nanocomposite hydrogel

Table 2.

Sample code		Substituent ratio					
	CMTKG	BSA	ACRYLAMIDE	ACRYLIC ACID	NPs	MBA	KPS
B3	0.3g	0.3g	0.4g	20µl	-	0.020g	0.028g
B3NP5	0.3g	0.3g	0.4g	20µl	5mg	0.020g	0.028g
B2NP10	0.3g	0.3g	0.4g	20µl	10mg	0.020g	0.028g
B3NP20	0.3g	0.3g	0.4g	20µl	20mg	0.020g	0.028g

2.6. Preparation of drug loaded hydrogel

The CFX solution was prepared by adding 20mg CFX into 10ml distilled water. The prepared hydrogel's pellets were then added into the solution for 24 hr for in vitro drug loading. Those drug loaded pellets were left for drying in an incubator at 35°C [47]

CHAPTER 3

EXPERIMENTAL SECTIONS

3.1 Swelling Studies

Fabricated hydrogels were tested for swelling in buffer solution at pH 7.4 and pH 1.2 for a period of 24h. The dried hydrogel discs were carefully weighed prior to soaking in the different solutions. After 1 hour, each hydrogel disc was removed and excess water was gently blotted off with filter paper and the discs were reweighed. The discs were then returned to the solutions. The procedure was repeated three times to obtain accuracy. The method used to conduct swelling studies was gravimetry method.

W_s = swollen hydrogel's weight

W_d= initial dry weight of the hydrogel

$$\text{Swelling Ratio } (\%) = \frac{(W_s - W_d)}{W_d} \times 100 \quad (1)$$

3.2 Ciprofloxacin loading and entrapment efficiency

The highest swelling was observed in B3, so therefore, the drug loading for the formulation was performed. The CFX-loaded CMTKG/BSA/PAM/AA/CuO bionanocomposite hydrogel was made as described in section 2.5. The Drug entrapment efficiency (DEE %) was calculated for the CFX-loaded nanocomposite hydrogel during the drug entrapment efficiency tests. A hydrogel sample was immersed in a drug solution for 24h, and its absorbance at λmax 279 nm was measured using UV-Vis spectrophotometer (Model: Cary UV-Vis). The amount of drug loaded was determined by Beer-Lambert law[48], [49]

Formula used for calculation of entrapment efficiency: -

$$DEE(\%) = \frac{Amount\ of\ drug\ laoded\ in\ hydrogel}{Initial\ amount\ of\ drug\ added\ in\ hydrogel} \times 100 \quad (2)$$

3.3 In vitro Ciprofloxacin release

In vitro study of the CFX-loaded CMTKG/BSA/PAM/AA/CuO bio-nano composite hydrogel was carried out in an orbital incubator shaker with pH 2.2 and pH 7.4 buffer solutions. The specific quantity of CFX loaded hydrogel pellets was placed in 200 ml of each buffer solution and incubated at 37°C. After 1 hour, 3ml of this solution was removed and replaced with 3ml of fresh buffer. The absorbance of the solution was then taken using a UV spectrophotometer (Model: Cary 300 UV-Vis) at λmax 279nm. The amount of drug was determined from calibration curve and entire process repeated for 24 hr.

3.4 Kinetic modeling of Ciprofloxacin

Drug release mechanisms were ascertained using a variety of mathematical models, including Korsmeyer-Peppas, Higuchi, Zero-order, and First-order models. The model with the regression coefficient (R2) value closest to 1 was considered the best fit after the values were compared.

CHAPTER 4

FABRICATION METHOD AND PROCESS

4.1 UV-Visible Spectroscopy (UV-Vis)

Optical spectroscopy is a physical method used to analyze different kinds of solvents and materials. It uses light in the visible, ultraviolet, and near-infrared spectrums. It is based on the Beer-Lambert law, which asserts that a solution's absorbance is directly correlated with both the path length and the concentration of the absorbing species in the solution.

4.1. UV-Vis Spectroscopy Principle: A molecule or an ion will undergo an electronic transition when it absorbs radiation. As a result, when a sample absorbs ultraviolet or visible light, the molecules' electronic states change. Electrons will be promoted from their ground state orbitals to higher energy excited state or anti-bonding orbitals by the light's energy. Three different kinds of ground state orbitals could be at play.

1. σ (Bonding) molecular

2. π (Bonding) molecular orbital

3. n (non-Bonding) atomic orbital.

Furthermore, the transition may involve two types of anti-bonding orbitals:

i. σ* orbital.
ii. π* orbital.

n* anti-bonding orbitals do not exist because n electrons do not form bonds. Thus, absorption of ultraviolet and visible light may cause the following electronic transitions.[50]

- σ to σ*
- n to σ*
- n to π*
- π to π*

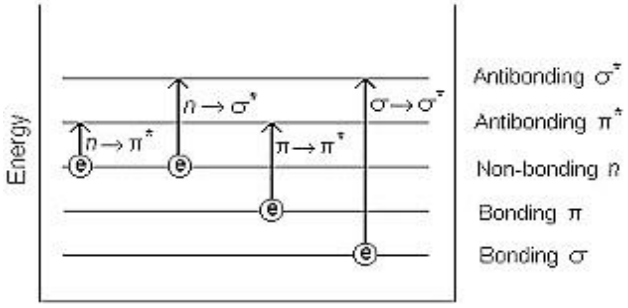

Fig 4.1: Possible Electronic Transitions

4.1.2 Beer Lambert's Law

The absorbance of light by a solution of an absorbing substance is proportional to the concentration of the absorbing substance and the path length, according to the Beer-Lambert law, also called the Bouguer-Beer law.

$$Log\ \frac{I}{I^{\circ}} = A = \varepsilon cl \qquad (4)$$

I° = intensity of the incident radiation
I = intensity of the attenuated radiation
A= absorbance
C= concentration
l= path length
ε= molar extinction coefficient [51]

4.1.3 Instrumentation

There are two types of absorbance:

a. **Single beam UV-Vis spectrophotometer**- To analyze one wavelength at a time, the single beam instrument (Figure 2) places a filter or monochromator between the source and the sample.. Only one beam goes through the sample compartment, and the user has to take measurements of the light intensity (reflected from the reference) before and after the sample is placed in the sample compartment.
b. **Double beam UV-Vis spectrophotometer-** In the double beam spectrophotometer, One beam passes through the sample while another beam passes through the reference. A researcher can simultaneously measure the reference standard and the sample.[52]

Components of the instrument :

1. Light source
2. Monochromator
3. Sample cell
4. Detector

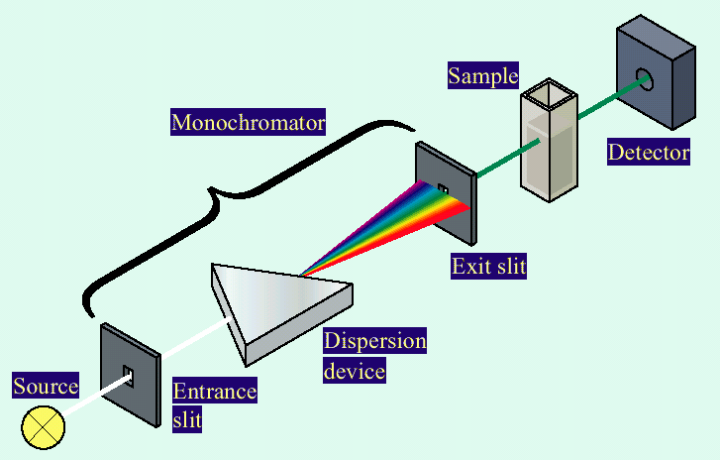

Fig 4.2 Single Beam UV-Vis spectrophotometer

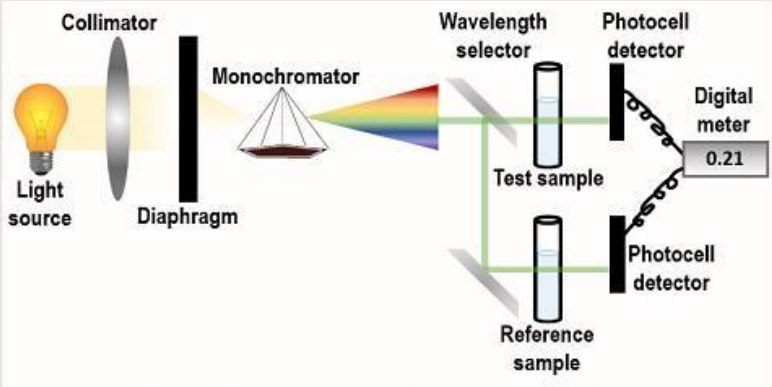

Fig 4.3 Double Beam UV-Vis spectrophotometer

4.2 Attenuated Toatl Reflection-Fourier Transform Infrared Spectroscopy (ATR-FTIR)

Functional groups, chemical bond and molecular structure of inorganic and organic compound is determined by Fourier transform infrared spectroscopy. FTIR principle works on the following process::

4.2.1 Principle of FTIR :

Modern IR spectroscopic instruments frequently employ the FTIR design in order to expedite the scanning and data collection process. The Michelson interferometer is the fundamental part of the FTIR spectrometer. Fig. 4.4 shows the ATR-FTIR spectrometer's detailed optical layout as well as the methods used to generate the IR spectrum. This apparatus creates the path difference in the infrared beams (emitted from an infrared light source) using a central beam splitter, two stationary and motorized optical mirrors, and an effective detector system. The most popular infrared source for producing infrared beams in FTIR instruments is silicon carbide rod, sometimes referred to as a globar source.The beam splitter divides the infrared beam from the source and directs it toward the motorized and stationary mirrors. Think about the beam that the motorized moving mirror reflects.

It introduces the path difference between this beam and the second beam (from the stationary mirror). These infrared beams have varying path lengths and are susceptible to both constructive and destructive interference. A DTGS (deuterated triglycine sulfate) detector gathers the output as a Fourier transform spectra of the sample response after this recombined infrared radiation interacts with the sample assembly.[53]

4.2.2Instrumentation:

FTIR spectrometer is made up of several components:

a. broadband IR source
b. sample compartment
c. Interferometer
d. Detector.

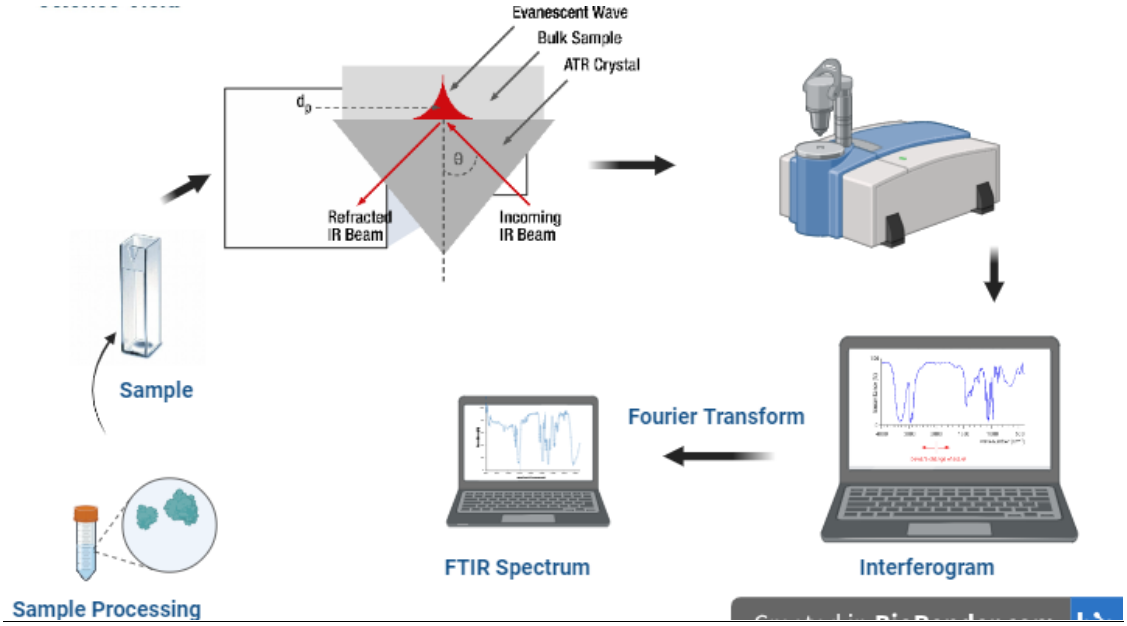

Fig 4.4 FTIR Spectrophotometer

4.3 Field Emission Electron Microscopy (FESEM)

Field emission scanning electron microscopy (FE-SEM), a cutting-edge technique, was used to capture the microstructure image of the materials. Since gas molecules scatter the primary beam and the secondary electrons emitted by the surface under investigation to disrupt the imaging beam, it is generally required to perform FE-SEM in a high-vacuum environment. Particulate materials' general shape, surface roughness, structure, and chemistry can all be more accurately described using FESEM.[54]

4.3.1 Principle:

The electron beam, after being focused by electromagnetic lenses, is scanned and reflected by the surface of the specimen and the reflected electrons (or interact with the specimen) form an image of the sample surface and topography.[55]

4.3.2 Instrumentation:

The FESEM uses-

a) **Field emission gun**- It produces highly concentrated high and low energy electron beams that significantly enhance spatial resolution and allow work to be done at very

low potentials (0.02-5 kv). This helps to prevent damage to electron beam-sensitive samples and minimize the charging effect on non-conductive specimens.

b) **In-lens detectors**- These detectors are necessary to get the best results from the equipment because they are made to function at very low acceleration potential and high resolution.[56]

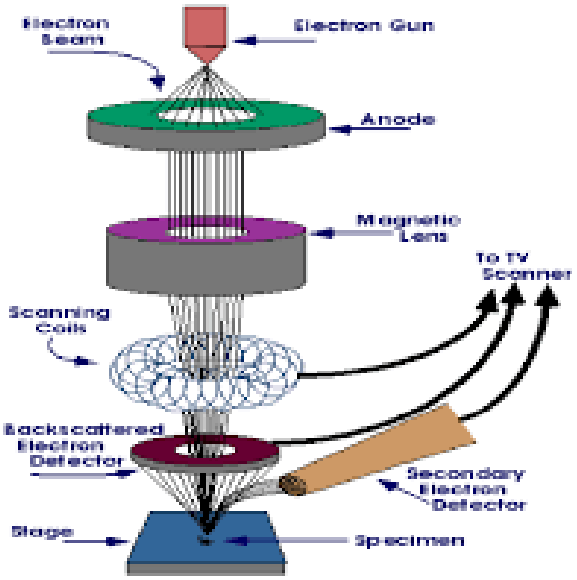

Fig 4.5 Schematic representation of FESEM

4.4 Powder X-Ray Diffraction (PXRD)

Determine the crystal phases, lattice plane spacing, size of crystal existence, preferred orientation, and epitaxial growth of the crystallites in order to examine the crystal content. A database of diffraction patterns can be used to identify materials and compounds because each material has a distinct diffraction pattern.

4.4.1Principle:

The second one (reflection) is more usual. When the conditions are met which allow the X-ray beam to interfere, the interaction between sample and the X-ray beam creates intense reflected X-rays as a result of constructive interference following Bragg's law.[57]

Bragg's Law-

$n\lambda = 2d\sin\theta$ (5)

n=integer
λ=wavelength
d= interplanar spacing.

4.3.3 Instrumentation:

A high resolution Bruker D8 diffractor was used to study the crystalline phases present of the sample using a Cukα radiation (λ=1.5406 0A) between 2θ range of 10-700C.

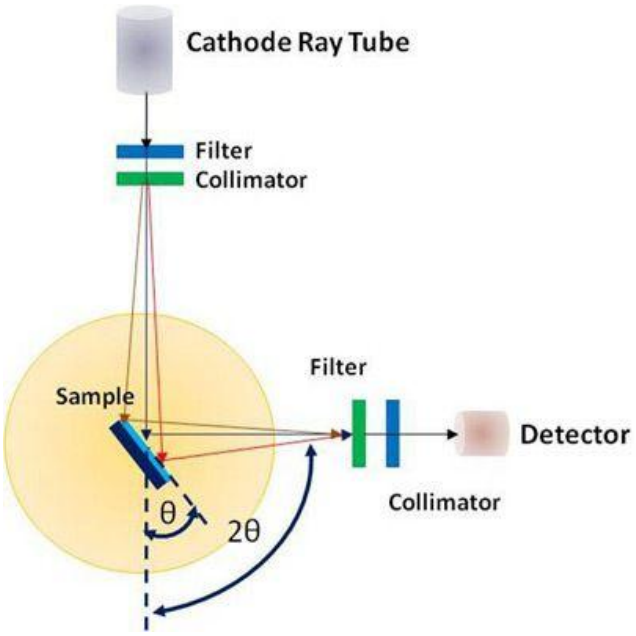

Fig 4.6 Showing Powder X-Ray Diffraction

CHAPTER 5

CHARACTERIZATION TECHNIQUES

5.1 ATR-FTIR Spectroscopy-

The ATR-FTIR spectra of CMTKG, AAM, BSA, CuO NPs, composite hydrogel and Nanocomposite hydrogel is Fig 5.1. In CMTKG, the broad band observed at 3300 cm^{-1} due to -OH stretching vibration. The peak at 1600 cm^{-1} observed due to asymmetric vibration of COO^- moiety [58]. The spectrum of AAM indicated the presence of NH_2 group in amide and carbonyl functional groups indicated by the peaks observed at 3345 cm^{-1} and 1668 cm^{-1} respectively [59]. The sharp peak at 1425 cm^{-1} indicates the presence of vinyl group. The BSA spectrum shows three characteristic bands: (i) the sharp Amide I band at 1646 cm^{-1}, indicates the presence of carbonyl group; (ii) the Amide II band at 1525 cm^{-1}, shows the combination of N-H bending and C-H stretching in secondary amide groups; (iii) the Amide III band at 1425 cm^{-1} [60]. The FTIR spectrum of B0 hydrogel, peak at 3300 cm^{-1} is broaden due to Hydrogen bonding. This indicates the participation of -OH in Radical Polymerization. It suggests the formation of hydrogen bonding between hydroxyl groups of CMTKG and grafted poly (acrylamide-co-acrylic acid) chains.

The FTIR spectrum of lysine-coated CuO NPs shows peak at 3450 cm^{-1} that indicates presence of -OH stretching vibration. The band at 1010 cm^{-1} indicates the C-O stretching of alcoholic and phenolic compounds. The 671 cm^{-1} and 553 cm^{-1} bands correspond to the Cu-O stretching vibrations in monoclinic structure of CuO NPs [61]. The band at 3300 cm^{-1} is due to the stretching of N-H in amide groups of lysine. The characteristic band of N-H bending in amide is observed at 1560 cm^{-1} [62]. Thus, confirms the presence of lysine coating on the CuO NPs.

The FTIR spectrum of B3 hydrogel shows characteristic bands at 3456-3234 cm^{-1} attributed to overlapping of O-H and N-H stretching vibrations. This indicates strong hydrogen bonding among CMTKG, BSA, AAM, AA. The characteristic amide I and amide II bands are observed at 1651cm^{-1} and 1572 cm^{-1} respectively. This confirms the successful incorporation of BSA into the hydrogel network. The shift of the amide I band as compared to B0 along with some changes in hydroxyl and carboxylate regions suggests the enhanced hydrogen bonding and electrostatic interactions between BSA and grafted poly(acrylamide-co-acrylic acid). This confirms the formation of stable and interconnected CMTKG-g-poly(acrylamide-co-acrylic acid)/BSA hydrogel network.

The FTIR spectrum of nanoparticles-loaded hydrogel show absorption band at 1214 cm^{-1}, attributed to C-N stretching vibrations of amide groups from BSA and polyacrylamide and contribution of lysine amino groups, coating the CuO NPs.

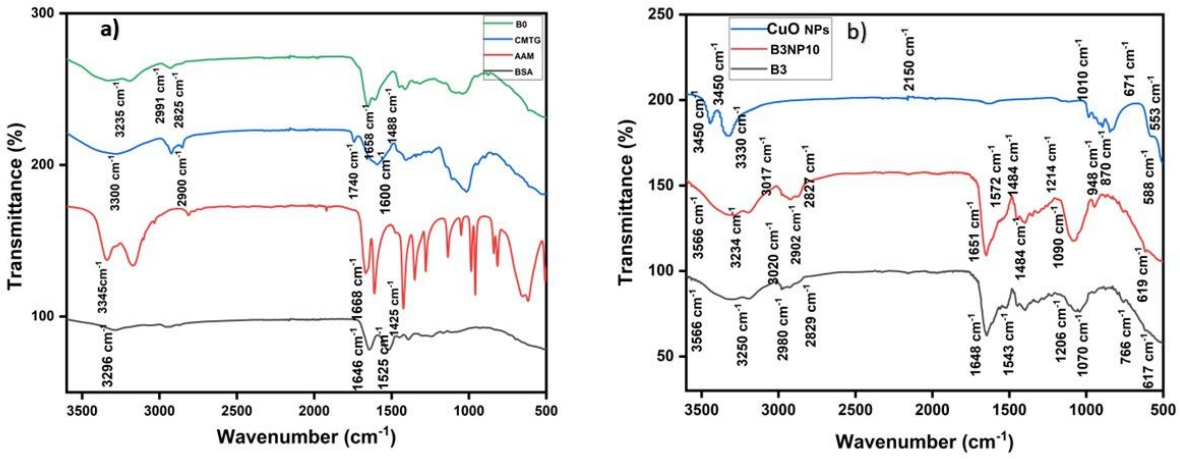

Fig 5.1 FTIR Spectra of a) B0, CMTKG, AAM, BSA b) Lysine-coated CuO bio-nanoparticles, B3NP10, B3

5.2. PXRD-

The Debye-Scherrer equation was utilized to estimate the crystalline size of 26.23±2.95 nm for CuO NPs . The PXRD pattern of the lysine-coated CuO bio-nanoparticles shows several intense and sharp diffraction peaks, pointing the crystalline nature of the prepared CuO nanoparticles. The prominent peaks observed at 2θ of around 35°, 38°, 48°, 58°, 61°, 66° and 68° are of the characteristic monoclinic phase of CuO, which is the desired phase of the product. The fact that the crystallite size is less than 100 nm indicates that the biosynthesized CuO NPs are nanocrystalline. [63]. This confirms that the synthesized nanoparticles possess a monoclinic structure and consist of a single-phase CuO [64]

By contrast, the nanocomposite hydrogel presents a broad diffuse hump with low peak intensity, suggesting the presence of mainly amorphous polymeric hydrogel matrix.[45] The diffraction peak intensity and peak width of CuO decreased, indicating successful dispersion and encapsulation of CuO bionanoparticles into the crosslinked polymer network without changing the crystal structure of CuO, because the crystal structure of CuO remained the same even after the incorporation of CuO bionanoparticles into the hydrogel. This indicates that the nanocomposite is now stable and has good compatibility between the polymer matrix and embedded CuO bionanoparticles.[65]

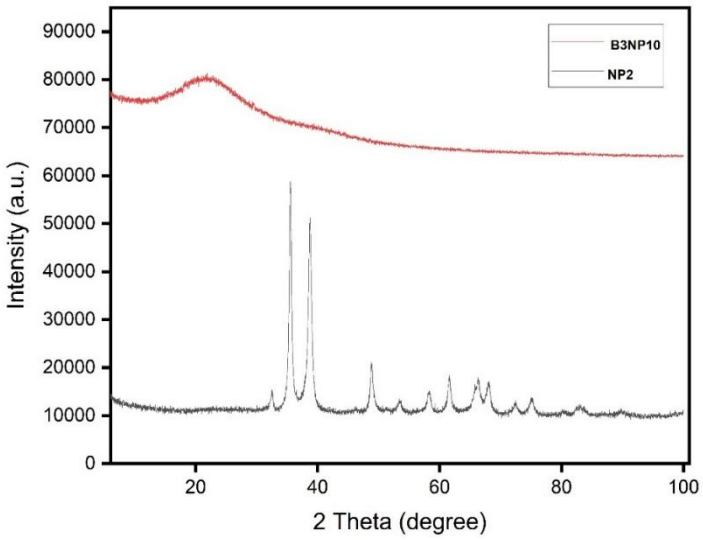

Fig 5.2 PXRD pattern of CuO bio-nanoparticles and nanocomposite hydrogel.

5.3. FESEM

FESEM image of the CuO NPs, composite Hyrogel and Bio-nanocomposite hydrogel are displayed in fig 5.3.

The lysine coated CuO bionanoparticles have rod and flake-like shape as shown in the image. It is seen that these flaky shaped morphology arised due to assembly of rods shaped particles [66]The nanoparticles appear to be clustered together, forming a porous and interconnected network. The elongated structures (with sharp edges and rough surfaces) are observed, showing good crystallinity of the CuO nanoparticles. Surface morphology shows high aggregation of the nanoparticles which is common with the metal oxide nanoparticles synthesized biologically because of intermolecular interactions and high surface energy. The lysine coating is play a role a stabilizing and capping agent and participates in the process of forming the nanoscale structure. [67]

The composite hydrogel reveal the continuous, uniform and homogeneous surface, suggesting that the CMTKG, BSA and PAM has blended successfully and cross linked together in the hydrogel matrix [68] . A number of micropores and voids can be seen scattered with the surface in small circular dark areas. The presence of pores represents a medium porosity.

The Bio-nanocomposite hydrogel shows a surface with compact, rough and heterogeneous, closely connected ridge-like and granular features. The pore size and surface roughness and surface roughness of the hydrogels have increased with the addition of the CuO nanoparticles suggesting strong interactions between the polymeric matrix and nanoparticles. This suggests the ability of CuO nanoparticles to function as cross-linkers [69] . The surface is wrinkled and aggregated, and uniformly distributed domains of nanoparticles can be seen, which is an indication of a successful embedding of the CuO bionanoparticle in the hydrogel network [68].

The high density and texture of this architecture indicate better structural strength, higher surface area and possible use for biomedical applications like drug delivery systems. Thus, facilitate the effective encapsulation of CFX within the polymer matrix.

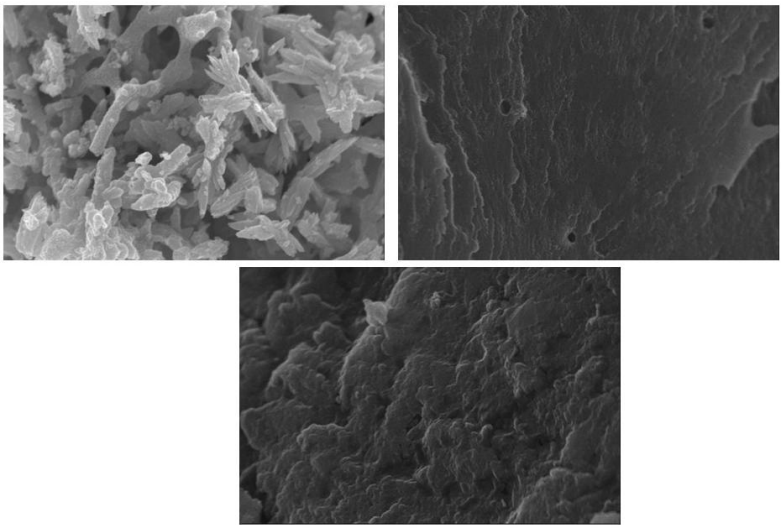

Fig 5.3: FESEM images at 30 KX magnification of (a) CuO NPs b) Composite Hydrogel) c) Bio-nanocomposite hydrogel

5.4. Cytocompatibility test

5.4.1 MTT Assay

The cytocompatibility was checked by MTT assay using L929 Fibroblast. The data of the CFX-loaded bio-nanoparticle composite hydrogel exhibits highly cytocompatible nature for the cells used in the study. The bio-nanocomposite CFX-loaded hydrogel showed low cytotoxicity with cell viability over 90% even at the higher concentrations from 50 to 250 µg. The viability values, however, are still above the accepted biocompatibility threshold which confirm the non-toxicity and bio-safety of the nanocomposite hydrogel. It is considered that a material with more than 75% of cell viability is non-cytotoxic[70].

Based on the results from these tests, the CFX-loaded nanocomposite hydrogel is found to be biocompatible and can be used in biomedical and drug delivery applications.

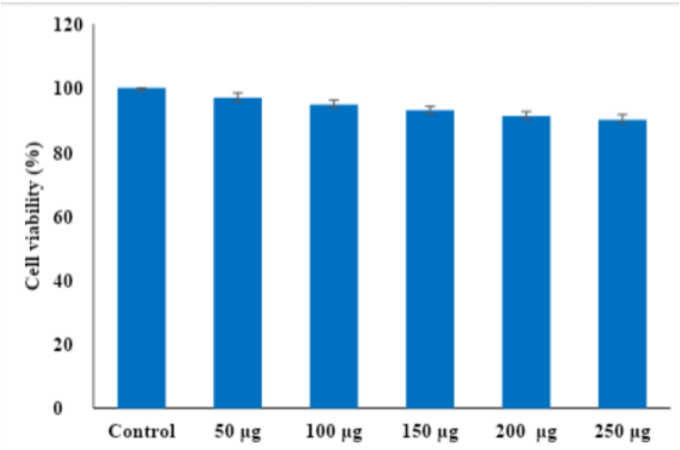

Fig 5.4.1 MTT Assay showing cell viability

5.4.2. Antibacterial Studies-

The results of the sample's antibacterial activity against various microbes using the disc diffusion method [71]. At a concentration of 100 µg/ml, The bare nanocomposite hydrogel sample showed inhibitory activity against Escherichia coli (9 mm) and Staphylococcus aureus (10 mm) at a concentration 100 µg/ml [72]

At 80 µg/ml concentration, the sample exhibited the antibacterial activity against all the tested bacteria, but it was more susceptible against Staphylococcus aureus (9 mm). [67]

The CFX-loaded nanocomposite hydrogel sample demonstrated inhibitory activity against Escherichia coli (10 mm) and Staphylococcus aureus (11 mm). The sample demonstrated antibacterial activity against all tested bacteria at a concentration of 80 µg/ml, but it was somewhat more vulnerable to Staphylococcus aureus (10 mm). [67] The sample's inhibitory effects on all of the strains used in this investigation increased as its concentration rose from 60 to 80 µg/ml. Thus, the CFX-loaded hydrogels showed considerable growth inhibition zones. This observation confirmed the release of ciprofloxacin from hydrogels.[73]

Samples	Concentrations (µg/ml)	Organisms/Zone of inhibition (mm)	
		Staphylococcus aureus	*Escherichia coli*
Samples	60	7	6
	80	9	7
	100	10	9
Standard (Std) (Amoxicillin)	10 µl/disc	13	11
DMSO	10 µl/disc	0	0

Fig 5.4.2a Showing Antibacterial Activity of bare Bio-nanocomposite hydrogel

Samples	Concentrations (µg/ml)	Organisms/Zone of inhibition (mm)	
		Staphylococcus aureus	*Escherichia coli*
Samples	60	9	8
	80	10	9
	100	11	10
Standard (Std) (Amoxicillin)	10 µl/disc	12	13
DMSO	10 µl/disc	0	0

Fig- 5.4.2b Showing Antibacterial activity of CFX-loaded bio-nanocomposite hydrogel.

5.5. Zeta Potential

Using Dynamic Light Scattering (DLS), the zeta potential of the CuO bio-NPs coated with lysine is displayed in Fig. 5.6. The high stability of the produced CuO NPs is indicated by the zeta potential, which was found to be –23 mV. According to reports, the nanoparticles' zeta potential is more stable when it is closer to −30 mV.[74]

Results

		Size (d.n...	% Intensity:	St Dev (d.n...
Z-Average (d.nm): 5966	Peak 1:	1752	100.0	185.7
PdI: 0.438	Peak 2:	0.000	0.0	0.000
Intercept: 0.955	Peak 3:	0.000	0.0	0.000

Result quality Refer to quality report

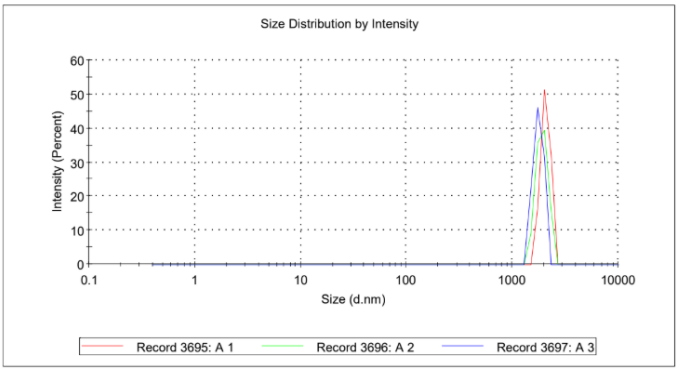

Fig-5.5 Shows Zeta Potential of CuO bio-nanoparticles.

CHAPTER 6

RESULT AND DISCUSSION

turnitin Page 37 of 48 - Integrity Submission Submission ID trn:oid:::27005:142438906

6.1 Overview of CMTKG-g-poly(acrylamide-co-acrylic acid)/BSA/CuO bio-nanocomposite hydrogel and CFX-loaded CMTKG-g-poly(acrylamide-co-acrylic acid)/BSA/CuO bio-nanocomposite hydrogel.

Developed hydrogel network is composed of carboxymethyl tamarind kernel gum (CMTKG), bovine serum albumin (BSA), acrylamide (AM), acrylic acid (AA) and lysine-coated copper oxide (CuO) nanoparticles. KPS was used as a free-radical initiator for the preparation of hydrogels. Thermal decomposition of KPS produces sulfate radical anions, which are able to initiate the polymerization of the acrylamide and acrylic acid monomers. The monomers undergo attack by these radicals to produce an increase in the length of growing polymer chains. This helps to graft the monomers onto the CMTKG backbone. As a result, a three-dimensional polymeric network is formed by the free radical polymerization. N,N′-Methylenebisacrylamide (MBA) was used as the chemical crosslinking agent. MBA has two polymerizable vinyl groups which are involved in free-radical polymerization reaction [75]. When forming the network, each vinyl group will bind to different growing polymer chains, which will form covalent bonds between the polyacrylamide chains and the poly(acrylic acid) chains. These covalent crosslinks will create a permanent three-dimensional network structure and impart a high level of mechanical stability and structural integrity to the hydrogel.

CMTKG is the backbone of the hydrogel and is the polysaccharide with a large number of hydroxyl (-OH) and carboxymethyl (-CH_2COOH) groups. The hydroxyl groups permit many sites for hydrogen bonding between molecules and the carboxymethyl groups give the polymer chain a negative charge once it is ionised. Acrylamide polymerizes by free radicals to produce polyacrylamide (PAM) that contains amide (-$CONH_2$) groups. PAM and CMTKG can engage in many hydrogen-bonding interactions, such as carbonyl oxygen with hydroxyl and amide nitrogen with carboxyl. These interactions provide network stabilization and increase the mechanical strength of the hydrogel network [76].

Acrylic acid also polymerises to form poly(acrylic acid), (PAA) which adds many carboxylic acid (-COOH) groups to the network. Under physiological and alkaline pH, some of these groups become partially charged, to form carboxylate (-COO^-) ions [77] . The carboxyl groups of PAA form strong hydrogen bonds with hydroxyl groups of CMTKG and amide groups of PAM, forming an interconnected polymeric network. Chemically crosslinked CMTKG-g-poly(acrylamide-co-acrylic acid) network is formed as a result of the combination of KPS and MBA. The bovine serum albumin and lysine coated CuO nanoparticles then enter into the

hydrogel matrix through hydrogen bonding, electrostatic interactions, metal-coordination and physical entanglement.

The bovine serum albumin (BSA) is a multifunctional bioactive component inside the hydrogel. The amino acid residues of BSA contain amino ($-NH_2$), carboxyl (-COOH), hydroxyl (-OH) and thiol (-SH) groups. The positive charged amino groups on BSA can form an electrostatic interaction with the negative charged carboxylate groups on the CMTKG and PAA chains. At the same time, hydrogen-bonding interactions occur between the hydroxyl and carboxyl groups of BSA, PAM and CMTKG. These interactions help in the incorporation of BSA into the polymeric network and in enhancing the biocompatibility of the hydrogel.

The addition of lysine-coated CuO nanoparticles further strengthens the hydrogel structure. The molecules of lysine are bound to the surface of CuO, leaving amino and carboxyl functional groups to the polymer matrix [78]. Lysine's carboxylate groups bind to the surface copper ions, creating a stable coating around the nanoparticles. The free amino groups of the lysine then undergo electrostatic interactions with CMTKG and PAA, as they are negative. Moreover, hydrogen bonding between the amino groups of lysine and the hydroxyl groups of CMTKG and between amide groups of PAM also occurs.

Ciprofloxacin was incorporated in the CMTKG-g-poly(acrylamide-co-acrylic acid)/BSA/CuO bio-nanocomposite hydrogel by hydrogen bonding, electrostatic interaction, protein-drug interaction and metal coordination. Hydrogen bonding between carboxyl and ketone groups of ciprofloxacin and hydroxyl, amide and carboxyl groups of CMTKG, PAM, PAA and BSA resulted. Moreover, the piperazine nitrogen of ciprofloxacin was involved in electrostatic interactions with the negatively charged carboxylate groups of the hydrogel network. For further improvement of drug loading and retention in the hydrogel matrix, strong chelation of CuO nanoparticles with Cu2+ ions was applied on lysine coated CuO nanoparticles [79]. The collective interactions resulted in an efficient drug encapsulation and sustained drug release behaviour.

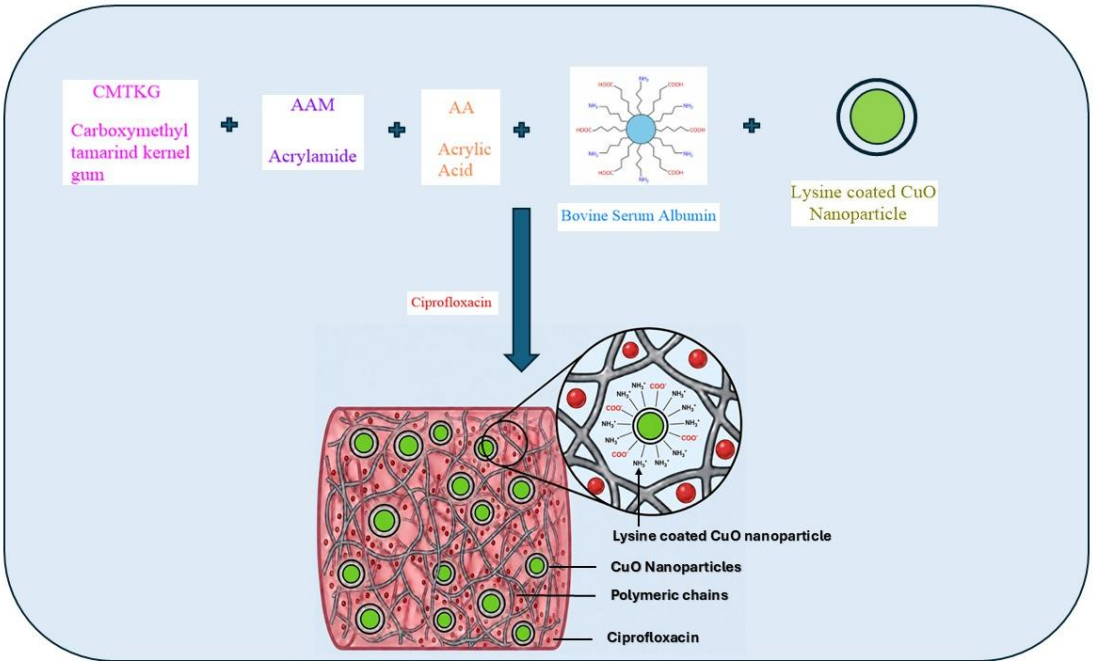

Fig 6.1 Diagram showing CFX- loaded nanocomposite hydrogel

6.2 Swelling Studies

All the synthesized hydrogels were subjected to swelling analysis in both pH 7.4 and pH 2.2. It was found that there was a significant increase in swelling at pH 7.4 as compared to swelling at pH 2.2. The three major factors that are usually responsible for the swelling of hydrogels are (i) the creation of inter-molecular voids inside the three-dimensional (3-D) network structure (ii) the porosity of the hydrogel surface (iii) the presence of hydrophilic moiety in the hydrogel matrix.[80]. The anionic carboxylate groups are abundantly present in the overall hydrogel network as these are present in CMTKG and Acrylic acid. The main reasons for the higher swelling of the corresponding hydrogels at ph 7.4 were the presence of hydroxyl groups that are hydrophilic and the electrostatic interaction force of the anionic carboxylate groups, and the osmotic pressure generated inside the hydrogels by the presence of the anionic carboxylate groups These physical interactions may increase the number of crosslinking points, which would raise the crosslink density and, in turn, decrease the hydrogels' pore sizes for water absorption.[73]

6.2.1 Impact of BSA-

The BSA concentration had a significant impact on the hydrogels' swelling (Fig. 6.2). Table 1 illustrates that the synthesized hydrogel (B0) without BSA and NPs exhibits greater swelling than all other samples. As the BSA concentration increased (from 0g to 0.3g), the swelling capacity decreased because the polymeric network's free volume decreased as physical interactions increased, increasing the cross-linking density. Increasing the BSA concentration resulted in a significant reduction in swelling at both pH 7.4 and pH 2.2. This is because the BSA acts as a cross-linker of polymer chains [81]

6.2.2 Impact of CuO NPs-

While varying concentrations of NPs (10–20 mg) are investigated for swelling, the concentration of BSA is maintained at 0.3 g. The swelling ratio initially decreases with an increase in NPs content up to a maximum of 20 mg. However, as the hydrogel network's cross-linking increased, it was discovered that this decreased as the Nps increased. Consequently, the swelling is reduced. This may be explained by CuONPs' knot-tying functions, which prevent polymer chains from growing longer. The chelation of certain hydroxyl and amine groups in the hydrogel networks with CuO nanoparticles may be the cause of CuONPs' knot-tying ability [82]. CuO NPs are cytotoxic and it was found that cell viability is concentration dependent with CuO NPs [83].

The surface charge of CuO nanoparticles is negative and the surface charge of Lysine is positive with amine charge, prefers to bind to the surface of CuO nanoparticles in preference to its carboxyl groups [84]. Hence, the positive amino acid coating to the NPs which increased their stability which was achieved by adding Lysine. [44]

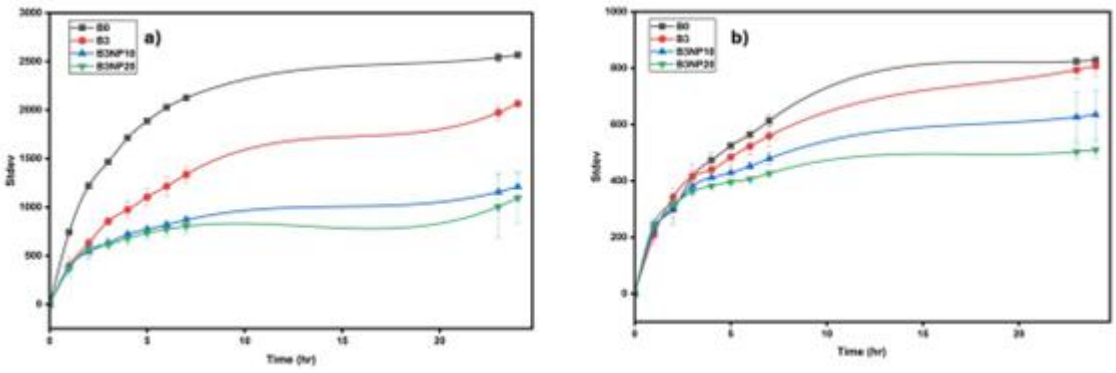

Fig 6.2: a) Swelling Ratio of B0, B3, B3NP10, B3NP20 at 7.4 pH b) Swelling Ratio of B0, B3, B3NP10, B3NP20 at 2.2 pH.

The above fig 6.2 shows the effect of concentration of both BSA and NPs on the Swelling Ratio from the hydrogels.

6.3 Loading of Drug and Encapsulation Efficiency

The drug loading and drug encapsulation efficiency of the CFX loaded composite and CFX-loaded nanocomposite hydrogel was studied. The DEE (%) and DLE (%) is shown in table mentioned below.

Table 3 DEE% and DLE% data table

Hydrogel Composition	Drug entrapement efficiency (%)	Drug Loading efficiency (%)
B0	37	7.7
B3	42	9.6
B3NP10	51.5	10.8
B3NP20	54.4	11.5

6.4 In vitro release of CFX

The in vitro investigation was performed on CFX loaded Lysine-coated CuO bio-nanocomposite hydrogel as shown in Fig. 6.2. Considerable amount of release of the drug was seen at pH 2.2 when compared with the release at pH 7.4. The drug release of 82%, 75% and 47% was observed in 24 h in alkaline medium (pH 7.4) for B3, B3NP10 hydrogel and B3NP20 hydrogel respectively. In acidic medium (2.2 pH), the drug release of 84% for B3 hydrogel, 74.9% for B3NP10 hydrogel, 59% for B3NP20 was found in 24h. In B0 hydrogel which is devoid of both BSA and NPs, showed drug release of 98% in both acidic and alkaline pH. Hydrogels swell more in basic media, but the drug release percentage is higher in acidic media. The solubility behaviour of CFX with respect to pH, which decreases in the pH range of 2.2 to 7.4 and increases in acidic pH, can account for the higher release percentage of the model drug. [85].

This observation suggests that the release of the drug from the drug loaded nanocomposite hydrogel is pH dependent.

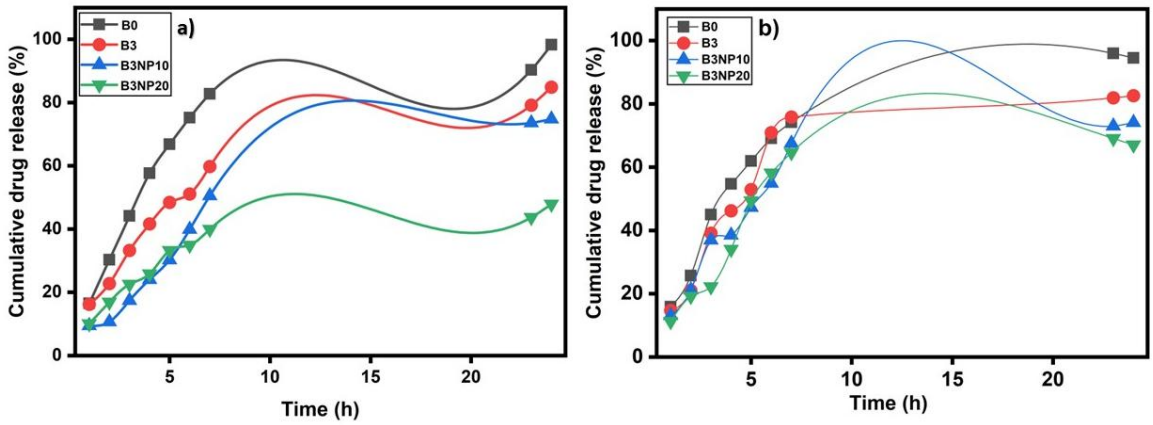

Fig 6.4: a) Drug Release of B0, B3, B3NP10, B3NP20 at 7.4 pH b) Drug Release of B0, B3, B3NP10, B3NP20 at 2.2 pH.

The above fig 6.4 shows the effect of the concentration of both BSA and NPs on the drug release from the hydrogels.

6.5 In vitro Antibacterial activity against E.coli and S.aureus

The Bio-nanocomposite hydrogel sample showed inhibitory activity against Escherichia coli (9 mm) and Staphylococcus aureus (10 mm) at a concentration 100 µg/ml.

The CFX-loaded bio-nanocomposite hydrogel sample showed inhibitory activity against Escherichia coli (10 mm) and Staphylococcus aureus (11 mm) at the same concentration as of above. The sample demonstrated antibacterial activity against all tested bacteria at a concentration of 80 µg/ml, but it was somewhat more vulnerable to Staphylococcus aureus in both cases [67]. i.e. (9 mm for bio-nanocomposite hydrogel and 10 mm for CFX-loaded bio-nanocomposite hydrogel).

Patients with osteomyelitis typically had S. aureus and E. coli. In this context, the ciprofloxacin-loaded bio-nanocomposite hydrogels, antibacterial properties against Gram-positive S. aureus and Gram-negative E.coli bacteria were slightly more susceptible to antibacterial activity from the bare bio-nanocomposite hydrogels. The hydrogels loaded with ciprofloxacin displayed significant growth inhibition zones. The release of ciprofloxacin from hydrogels was confirmed by this observation. The results showed that the hydrogels loaded with CFX may be a promising treatment option for osteomyelitis.[73]

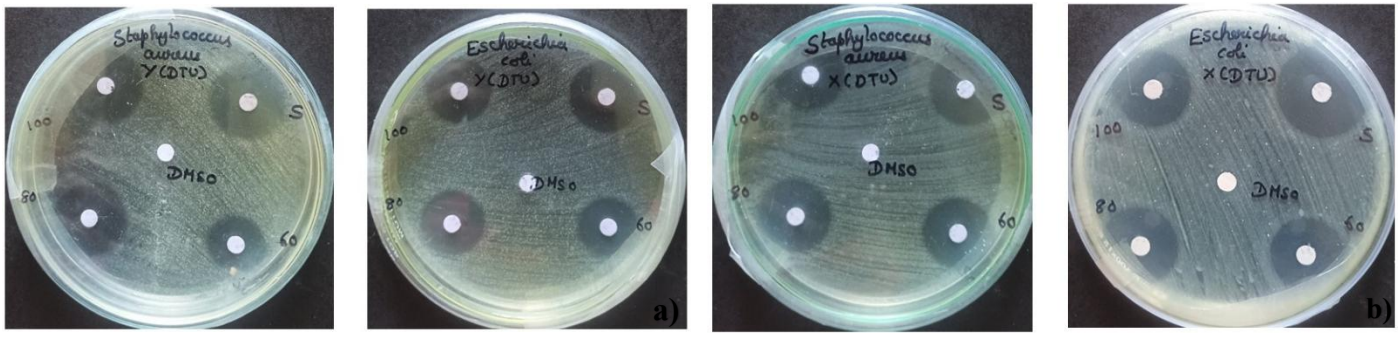

Fig 6.5. Showing Antimicrobial activity against S. aureus and E. coli by a) Bio-nanocomposite Hydrogel b) CFX-loaded Bio-nanocomposite Hydrogel.

6.6 Kinetic Modelling of Ciprofloxacin

The drug release Kinetics of CFX suggests Kormeyer-Peppas model as best described fit for both pH conditions. At pH 7.4, the release of ciprofloxacin from B0, B3, and B30 formulations with R^2 values of 0.9998, 0.9892, and 0.8692, respectively. The release exponent values (n = 0.4521–0.9019) indicate a transition from Fickian diffusion to non-fickian and near Case-II transport. B0 shows n= 0.902 which is less than unity and B3 with n= 0.686 which is greater than 0.5. Here, the release is contributed by non-fickian mechanism because the n values is >0.5 and <1 for these formulations [85]. The nanocomposite hydrogel (B3NP20) follows Fickian diffusion mechanism since n= 0.452 i.e. $n \leq 0.5$ [86] The results suggests that both drug diffusion and polymer relaxation contribute to the release process. But in nanocomposite hydrogel only Drug diffusion is responsible for drug release process. Whereas for 2.2 pH condition, the release exponent values (n = 0.807–0.922) indicate that drug release is controlled by non-fickian mechanism, indicating both drug diffusion and polymeric chain relaxation are responsible for drug release process [87].

Table 4 Different Kinetic Models used for evaluation of drug release

Model	Equations	Reference
Zero Order	$W_t = W_\infty + k_0 t$ k_0 = zero-order constant	**[88]**
Higuchi	$W_t/W_\infty = k_{HG} t^{1/2}$ k_{HG} = Higuchi constant	[37]
First Order	$\text{Log } W_t = \text{Log } W_\infty + \frac{kt}{2.303}$ k = first order constant	**[89]**
Korsmeyer–Peppas	$W_t/W_\infty = kt^n$ k = kinetic constant n = diffusion exponent	**[90]**

Table 5 Kinetic modeling data of **CFX**-loaded CMTKG-g-poly(acrylamide-co-acrylic acid)/BSA/CuO bio-nanocomposite hydrogel at 7.4 pH.

Hydrogel Formulation	Zero Order		First Order		Korsmeyer peppas		Higuchi	
	R^2	K	R^2	K	R^2	K	R^2	K
B0	0.635	2.5122	0.8420	0.1262	0.832	23.65	0.78	17.69
B3	0.838	2.4340	0.9528	0.0646	0.940	15.53	0.934	16.33
B3NP20	0.6768	1.1817	0.732	0.017	0.812	13.16	0.812	8.232

Table 6 Kinetic modeling data of **CFX**-loaded CMTKG-g-poly(acrylamide-co-acrylic acid)/BSA/CuO bio-nanocomposite hydrogel at 2.2 pH.

Hydrogel Formulation	Zero Order		First Order		Korsmeyer peppas		Higuchi	
	R^2	K	R^2	K	R^2	K	R^2	K
B0	0.727	2.685	0.968	0.121	0.978	23.65	0.715	13.78
B3	0.601	2.261	0.742	0.060	0.96	13.85	0.744	15.99
B3NP20	0.576	0.576	0.650	0.038	0.955	10.23	0.715	13.78

CHAPTER 7

CONCLUSION

In the present study, a novel pH-responsive composite hydrogel (CMTKG/BSA/PAM/AA) loaded with phytogenically synthesized CuO nanoparticles that were coated with the amino acid lysine was successfully developed and characterized for controlled oral delivery of the antibiotic ciprofloxacin. The CuO nanoparticles were synthesized by an eco-friendly green synthesis route by using Catharanthus roseus (Madagascar periwinkle) leaf extract, and the hydrogel was synthesized by free radical graft polymerization by using CMTKG, BSA, acrylamide, and acrylic acid. The addition of BSA and CuO nano particles also enhanced the structural integrity and crosslinking density of the hydrogel network which led to less swelling of the hydrogel and thus prevented burst drug release. Swelling studies showed that the system was highly sensitive to pH and the pH 7.4 showed a high swelling and the acidic pH showed a low swelling thereby making it suitable for oral drug delivery application. The optimized nanocomposite hydrogel demonstrated sustained and controlled release profile of ciprofloxacin, which agreed well with the Korsmeyer–Peppas kinetic model indicating Fickian drug release mechanism. The FTIR, PXRD and FESEM characterization studies validated the formation of the hydrogel, incorporation of CuO nanoparticles and the porous nature essential for the encapsulation and release of drug. The synthesized CuO nanoparticles were crystalline in nature and had a higher surface area and antibacterial activity due to their nanoscale size. Antimicrobial studies showed great inhibition against E. coli and S. aureus, thus confirming the synergistic antibacterial effect of the combinations of ciprofloxacin and CuO nanoparticles. Moreover, MTT assay indicated the excellent biocompatibility of the prepared hydrogel system with a cell viability of over 90%, an essential requirement for use in biomedical applications. Based on literature analysis of similar drug delivery systems made of hydrogel, it is found that the mechanical strength, drug encapsulation efficiency, antibacterial activity and controlled drug release behavior of the composite materials are improved with the addition of natural polysaccharides and synthetic polymers and metal oxide nanoparticles. The addition of CMTKG and BSA enhance the hydrophilicity, biodegradability and biocompatibility of conventional PAM-based hydrogels, while the antimicrobial activity and environmentally friendly synthesis process of phytogenic CuO nanoparticles provide an extra benefit.. In summary, the developed CMTKG/BSA/PAM/AA/CuO nanocomposite hydrogel exhibited promising ability to function as a controlled release drug delivery system, boasting the antibacterial activity as well as excellent cytocompatibility. The study accentuates the potential of the composite hydrogels prepared by the green synthesis of metal oxide nanoparticle for advanced applications in biomedical and pharmaceutical field. Further studies can be

conducted to evaluate the nanoparticles in vivo, to carry out long-term stability studies and to optimize the concentration of nanoparticles for targeted therapeutic applications.